CHINESE OPTICS LETTERS

Vol. 21, No. 5 | May 2023

Solar-blind avalanche photodetector based on epitaxial $Ga_2O_3/La_{0.8}Ca_{0.2}MnO_3$ pn heterojunction with ultrahigh gain

Ning Li (李 宁)[1], Qingyi Zhang (张清怡)[1], Yongtao Yang (杨永涛)[1], Yuanjun Tang (唐源骏)[1], Tao Zhang (张 涛)[1], Jiaying Shen (申佳颖)[1], Yuehui Wang (王月晖)[1], Fan Zhang (张 帆)[1], Yang Zhang (张 杨)[2,3*], and Zhenping Wu (吴真平)[1**]

[1] State Key Laboratory of Information Photonics and Optical Communications & School of Science, Beijing University of Posts and Telecommunications, Beijing 100876, China

[2] Institute of Modern Optics, Nankai University, Tianjin 300071, China

[3] Tianjin Key Laboratory of Micro-Scale Optical Information Science and Technology, Tianjin 300071, China

*Corresponding author: yangzhang@nankai.edu.cn

**Corresponding author: zhenpingwu@bupt.edu.cn

Received January 29, 2023 | Accepted March 10, 2023 | Posted Online April 6, 2023

Ga_2O_3-based avalanche photodetectors (APDs) have gained increasing attention because of their excellent photoelectric conversion capability in the UV solar-blind region. Integrating high-quality epitaxial Ga_2O_3 with p-type semiconductor remains an open challenge associated with the integration difficulty on alleviating its defects and dislocations. Herein, we construct an APD consisting of epitaxial β-$Ga_2O_3/La_{0.8}Ca_{0.2}MnO_3$ heterostructure. The pn junction APDs exhibit a high responsivity of 568 A/W as well as an enhanced avalanche gain of up to 3.0×10^5 at a reverse bias voltage of 37.9 V. The integration capability demonstrated in this work provides exciting opportunities for further development of high-performance Ga_2O_3-based electronics and optoelectronics.

Keywords: avalanche photodetector; Ga_2O_3; solar-blind; pn junction.

DOI: 10.3788/COL202321.051604

1. Introduction

Significant progress has been made in the development of solar-blind photodetectors (PDs) that operate in the ultraviolet (UV) wavelength range (200–280 nm) for a variety of applications, such as secure communication, missile guidance, environmental monitoring, UV astronomy, and position navigation[1–3]. Solar-blind PDs made of wide bandgap (WBG) semiconductors with bandgap (E_g) exceeding 4.4 eV have demonstrated great potential for replacing currently available commercial photomultiplier tube (PMT) PDs, which have limitations such as being bulky, fragile, and requiring Wood's filters to cut off the detecting wavelength[4]. To date, available WBG semiconductors include MgZnO ($E_g = 3.35$–7.8 eV, alloying)[5], AlGaN ($E_g = 3.4$–6.2 eV, alloying)[6], Ga_2O_3 ($E_g = 4.6$–5.3 eV, polymorph-dependent)[7], and diamond ($E_g = 5.5$ eV, fixed)[8]. Among them, Ga_2O_3 possesses several evident advantages, such as a suitable E_g for solar-blind sensing, high exciton binding energy (up to 40–50 meV at room temperature), a large breakdown electric field up to 8 MV/cm, excellent thermal, chemical, and radiation stability, plus the availability of scalable high-quality crystals and films, making it a building block for solar-blind PDs[9,10].

To date, Ga_2O_3-based solar-blind PDs have been fabricated with various device configurations, including the photoconductive[11–13], Schottky diode[14–16], heterojunction[17–19], and avalanche PD (APD)[20-23]. Compared with other types of PDs, APDs offer orders of magnitude higher responsivity and gain and are conceivably becoming the research hotspot of the field. All solid-state Ga_2O_3-based APDs allow low voltage operation and optical filter-free integration, promising more compact and robust solar-blind PDs. Through unremitting efforts, the performance metrics for reported APDs are being continually pushed in the direction of realizing high responsivity and avalanche gain. APDs work in a high reverse bias condition, so this allows avalanche multiplication of the charge carriers formed upon the UV photon impact. The photon-induced charge carriers are accelerated and undergo cascade amplifications through impact ionization with the electric field in the depletion region. APDs implemented using pn junctions are favored to form a broader depletion region. However, most reported Ga_2O_3-based APDs so far are made of n-n isotype heterojunctions, which take into account the intrinsic n-type nature of Ga_2O_3 and the associated band alignments[20–22,24]. Integrating high-quality epitaxial Ga_2O_3 with a p-type semiconductor layer

© 2023 Chinese Optics Letters

remains a promising approach to enhance the APDs' performance, but there are challenges associated with the integration difficulty on alleviating the defects and dislocations.

Orthorhombic perovskite manganites in the form of $Re_{1-x}Ak_xMnO_3$ (where Re and Ak are rare-earth and alkaline-earth ions, respectively) have raised considerable interest for their fascinating physical properties[25,26]. In manganite-based systems, the cross coupling between different degrees of freedom (structural, charge, spin, and orbital) gives rise to rich physical phenomena, such as colossal magnetoresistance, charge/orbital ordering, and electronic phase separation[27]. Especially, when the alkaline-earth ion is a divalent ion such as Ca^{2+}, Sr^{2+}, and Ba^{2+}, manganites exhibit hole-doped p-type semiconductor characteristics with considerable large hole carrier concentrations[25]. Meanwhile, with a compatible lattice constant, perovskite manganites could be used as excellent p-type materials to form a pn junction with Ga_2O_3[28]. In this study, we construct a solar-blind APD based on epitaxial β-Ga_2O_3/$La_{0.8}Ca_{0.2}MnO_3$ (LCMO) pn junction with ultrahigh gain and responsivity, which is approaching the benchmark of commercial PMTs. Moreover, perovskite manganites LCMO is an excellent p-type semiconductor promoting epitaxial growth of various perovskite functional oxides. The integration technology demonstrated in this work will be an important exploration in developing high-performance Ga_2O_3-based electronic and photonic devices.

2. Experiments

The commercial (001)-oriented $SrTiO_3$ (STO) single crystal (10 mm × 10 mm) was employed as the substrate. A 100 nm thick p-type LCMO layer was deposited using the pulsed-laser deposition (PLD) technique with the following parameters: a growth temperature of 700°C, an O_2 pressure of 20 Pa, a pulse energy of ~80 mJ, and a repetition frequency of 2 Hz. After deposition, the sample was annealed at 700°C under an O_2 pressure of 4×10^4 Pa for 30 min before natural cooling down. Squared patterns with an area size of 100 μm × 100 μm were defined using a room-temperature-grown amorphous STO layer via standard photolithograhy and lift-off procedure. A 300 nm thick Ga_2O_3 film was then deposited using magnetron sputtering with the following parameters: a growth temperature of 760°C, an Ar pressure of 1 Pa, and an RF power of 70 W. Then, 30 μm × 30 μm squared Au/Ti metals were sputtered on top of both the Ga_2O_3 and LCMO layers as the ohmic contact electrodes and were connected to a printed circuit board (PCB) using wire bonding. The schematic structure of the APD device is shown in Fig. 1. The crystalline quality of the sample was recorded by a Rigaku D/max2500PC X-ray diffractometer. A Hitachi U3900 UV-VIS spectrometer was used to examine the optical bandgap of the sample. A Keithley 4200 semiconductor characterization system was employed to investigate the current-voltage (I-V) characteristics. A commercial low-pressure UV lamp was employed as the 254 nm light source. The chemical bonding property was studied using a Thermo Scientific K-Alpha+ XPS system with a monochromated Al-Ka (energy of 1486.6 eV) X-ray source.

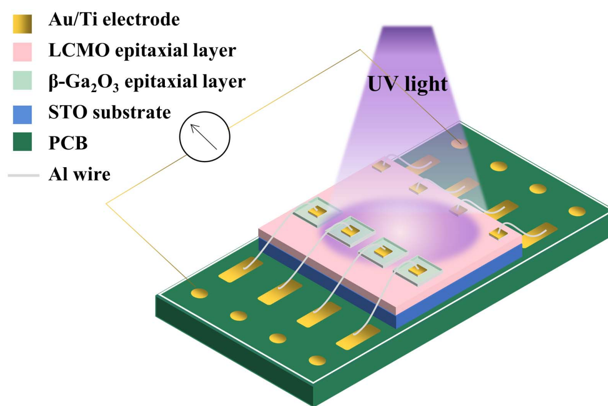

Fig. 1. Schematic structure of the β-Ga_2O_3/LCMO pn junction APD.

3. Results

Figure 2(a) shows the X-ray diffraction (XRD) patterns of the LCMO layer and Ga_2O_3/LCMO bilayer grown on STO substrates. The results indicate that the Ga_2O_3 layer is of the monoclinic β phase (ICSD No. 34243). In addition to the STO substrate peaks, both Ga_2O_3 and LCMO exhibit obvious (100)-oriented diffraction peaks. This suggests that the LCMO/STO and Ga_2O_3/LCMO/STO heterostructures are epitaxial in nature, with the crystal lattices of the different layers aligned with each other. If we consider the lattice compatible with oxygen atom spacings between the Ga_2O_3 and LCMO structures, the in-plane epitaxial relationship of the Ga_2O_3/LCMO/STO heterostructure is [001] Ga_2O_3//[011]LCMO//[011] STO, indicating a specific orientation rotation between each layer. The d spacing of the (400) plane of Ga_2O_3 is determined to be 3.017 Å from the peak position, slightly larger than the bulk value of 2.971 Å. This indicates that the Ga_2O_3 layer is under in-plane compressive strain due to lattice misfit. Figure 2(b) shows the cross-sectional view of the atomic-level arrangement of the β-Ga_2O_3/LCMO heterostructure interface, which is critical for the performance and functionality of the device.

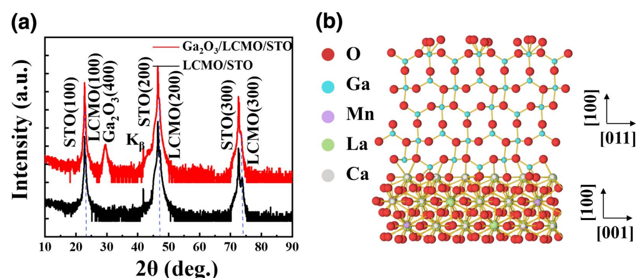

Fig. 2. (a) XRD patterns of β-Ga_2O_3/LCMO/STO (red line) and LCMO/STO (black line); (b) atomic diagram of cross section in the (100) direction of pn junction.

We then investigated the UV photoresponse performance of the APD with a Ga_2O_3/LCMO pn junction in detail. Figure 3(a) shows the *I-V* curves of the APD in the dark and under various intensities of 254 nm light, all of which exhibit typical rectification characteristics. As the light intensity increases from 1 to 100 μW/cm^2, the measured photocurrent presents an increasing trend. As shown in the inset of Fig. 3(a), the current increases as the light intensity increases, even at a high voltage of −37 V. The multiplication gain M reflects the device's ability to amplify the photocurrent through avalanche multiplication and represents an important figure of merit (FOM) for evaluating the performance of an APD. Thus, APDs endowed with a higher multiplication gain will be more effective for amplifying the photocurrent. It is defined as follows:

$$M = \frac{\text{Multiplied photocurrent}}{\text{Primiary unmultiplied photocurrent}} = \frac{I_p(V) - I_d(V)}{I_p(0) - I_d(0)}, \quad (1)$$

where $I_p(V)$ and $I_d(V)$ are the multiplied photocurrent and dark current, whereas $I_p(0)$ and $I_d(0)$ are the primary or unmultiplied photocurrent and dark current that are measured in the absence of multiplication, respectively[29]. The avalanche multiplication curve of the pn junction APD is derived from the dark current and photocurrent under 1 μW/cm^2 light irradiation. As shown in Fig. 3(b), both the dark current and the photocurrent are almost constant in the low reverse bias regime (< 6 V). We assume that this flat region is the unmultiplied region of the photocurrent curves, and therefore we take the unit gain $M = 1$ at $V = 6$ V. The reverse bias dependent on the corresponding M values is shown on the right axis of Fig. 3(b). With the reverse bias increasing from 6 to 20 V, the dark current remains below 10 pA, while the photocurrent shows a slightly increasing trend. Note that the avalanche breakdown onset bias is around 20 V, where both the dark current and photocurrents start to increase exponentially. The maximum M value for the Ga_2O_3/LCMO pn junction APD can reach an ultrahigh value of 3.0×10^5 at a reverse bias voltage of 37.9 V, which is among the highest values for recently reported Ga_2O_3-based APDs. The responsivity (R) is another critical FOM that reflects the PD's ability to generate photoexcited carriers and is calculated by $R = \frac{I_p - I_d}{P_\lambda S}$, where P_λ, S, I_p, and I_d represent the incident light intensity, effective irradiation area (the electrode area is ignored for the convenience of calculation), photocurrent, and dark current, respectively[1]. Figure 3(c) shows the light intensity-dependent photocurrent and responsivity of the Ga_2O_3/LCMO pn junction APD at a reverse bias of 20 V. The photocurrents exhibit a monotonic increase with increasing light intensity. A decrease in responsivity at higher illumination intensities is also observed. As the incident light power increases, the number of free electrons increases along with the enhanced carrier scattering rate. The springing free electrons also increase the probability of photoexcited electron–hole recombination, which inevitably impairs responsivity. The spectral selectivity of the APD is demonstrated in Fig. 3(d). It is worth noting that the device shows a significant response to light with $\lambda < 280$ nm, with a peak at ~255 nm, while the photoresponse with $\lambda > 280$ nm can be ignored, in agreement with the intrinsic absorption edge of Ga_2O_3. These results guarantee the obtained APD is solar-blind selective.

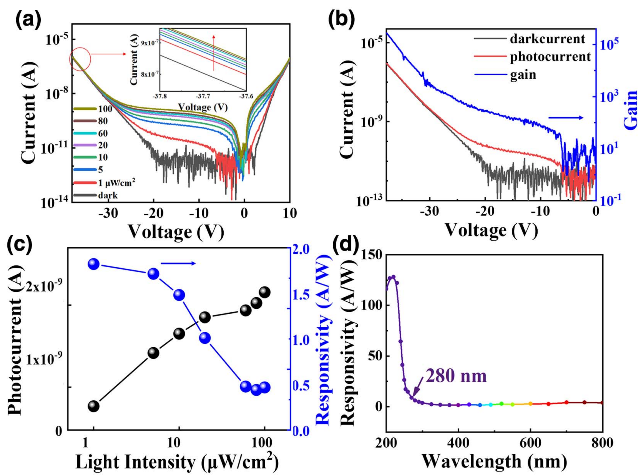

Fig. 3. Solar-blind photoresponse characteristics of Ga_2O_3/LCMO APD. (a) *I-V* curves (log scale) in dark and under different light illumination (1–100 μW/cm^2). The inset shows the *I-V* curves enlarged near −37 V. (b) Reverse *I-V* curves in dark and under 1 μW/cm^2 254 nm light intensity; the right axis shows the multiplication gain values. (c) The light intensity-dependent photocurrent and responsivity at a reverse bias of 20 V. (d) Photoresponse spectrum at a reverse bias of 30 V.

The external quantum efficiency (EQE) and linear dynamic range (LDR) are two other important FOMs for assessing the performance of the APD. The EQE is the ratio of the number of carriers produced by the PD to the number of incident photons: $\mathrm{EQE} = \frac{Rhc}{e\lambda}$, where R is the responsivity, h is Planck's constant, c is the speed of light, e is the electron charge, and λ is the incident light wavelength. The EQE can be used to evaluate the efficiency of a PD converting light into electrical charge. The LDR is defined as the ratio of the maximum to minimum detectable light intensity and is typically expressed in decibels (dB). An APD with a high LDR can accurately detect a wide range of light intensities, which is important in applications where the light intensity may vary over a wide range. It is calculated by $\mathrm{LDR} = 20\log(\frac{I_p}{I_d})$, where I_p and I_d are the photocurrent and dark current, respectively. The R, EQE, and LDR for the pn junction APD as a function of reverse bias are displayed in Figs. 4(a)–4(c). The maximum R, EQE, and LDR reached 568 A/W, 2.77×10^5%, and 83.3 dB, respectively. The obtained FOMs for pn junction APDs surpass those of reported Ga_2O_3-based photoconductive PDs[30,31] and rank among the best values for Ga_2O_3-based APDs[20–22,24].

4. Discussion

The photoresponse performance of an APD primarily determines its energy band alignment, specifically, the barrier height

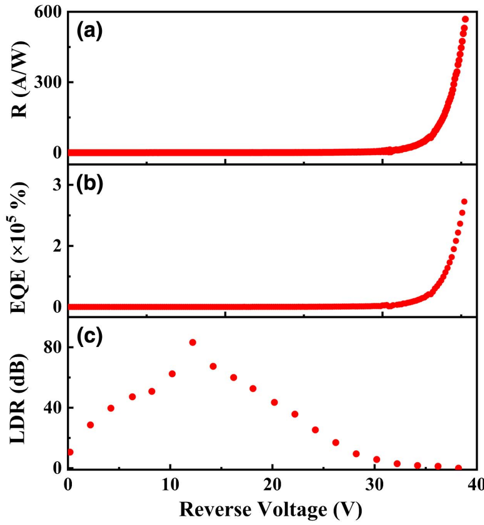

Fig. 4. (a) Responsivity; (b) EQE; and (c) LDR of Ga_2O_3/LCMO pn junction APD under 1 μW/cm^2 254 nm UV light intensity as a function of reverse bias.

(Φ_B), built-in potential, and band offsets (ΔE_c and ΔE_v)[32]. We conducted X-ray photoelectron spectroscopy (XPS) to explore the band diagrams of the Ga_2O_3/LCMO pn junction. To conduct high-resolution XPS study, we prepared three samples: LCMO(∼100 nm)/STO, Ga_2O_3(∼300 nm)/LCMO(∼100 nm)/STO, and Ga_2O_3(∼3 nm)/LCMO(∼100 nm)/STO. After calibrating the binding energy shift of the XPS spectra using the C 1s peak (284.8 eV), we applied Kraut's method to extract the band offsets of the Ga_2O_3/LCMO pn junction as follows[33]:

$$\Delta E_v = (E^{\mathrm{LCMO}}_{\mathrm{Mn^{3+}\,2p}} - E^{\mathrm{LCMO}}_{\mathrm{VBM}}) - (E^{\mathrm{Ga_2O_3}}_{\mathrm{Ga\,2p}} - E^{\mathrm{Ga_2O_3}}_{\mathrm{VBM}}) - (E^{\mathrm{LCMO}}_{\mathrm{Mn^{3+}\,2p}} - E^{\mathrm{Ga_2O_3}}_{\mathrm{Ga\,2p}}), \quad (2)$$

$$\Delta E_c = (E^{\mathrm{LCMO}}_g - E^{\mathrm{Ga_2O_3}}_g) - \Delta E_v. \quad (3)$$

In LCMO, Mn exists in different valence states (Mn^{3+} and Mn^{4+}). Mn^{3+} is the more dominant component and exhibits a more significant peak in XPS studies. Therefore, we used the Mn^{3+} $2p_{3/2}$ and Ga $2p_{3/2}$ core levels (CLs) of LCMO and Ga_2O_3, respectively, for the valence band offset calculations. Furthermore, we partially extrapolate the tangent line near the low binding energy position to intersect with the horizontal extension line and determine the valence band maximum at the intersection point. From Figs. 5(a)–5(c), we can obtain the values of 1114.34 eV, 640.18 eV, and 476.71 eV for $E^{\mathrm{LCMO}}_{\mathrm{Mn^{3+}\,2p}} - E^{\mathrm{LCMO}}_{\mathrm{VBM}}$, $E^{\mathrm{Ga_2O_3}}_{\mathrm{Ga\,2p}} - E^{\mathrm{Ga_2O_3}}_{\mathrm{VBM}}$, and $E^{\mathrm{LCMO}}_{\mathrm{Mn^{3+}\,2p}} - E^{\mathrm{Ga_2O_3}}_{\mathrm{Ga\,2p}}$, respectively. ΔE_v is calculated to be 2.55 eV according to Eq. (2). We performed UV-VIS absorption spectrum measurement on Ga_2O_3 and LCMO films, and the obtained data were processed using the Tauc plots method to obtain $(\alpha h\nu)^2$ versus $h\nu$, as shown in Figs. 5(d) and 5(e). By extrapolating Figs. 5(d) and 5(e), the E_g of Ga_2O_3 and LCMO are found to be 4.88 and 1.42 eV, respectively, which are consistent with previous studies[7,26]. By substituting these values into Eq. (3), we can

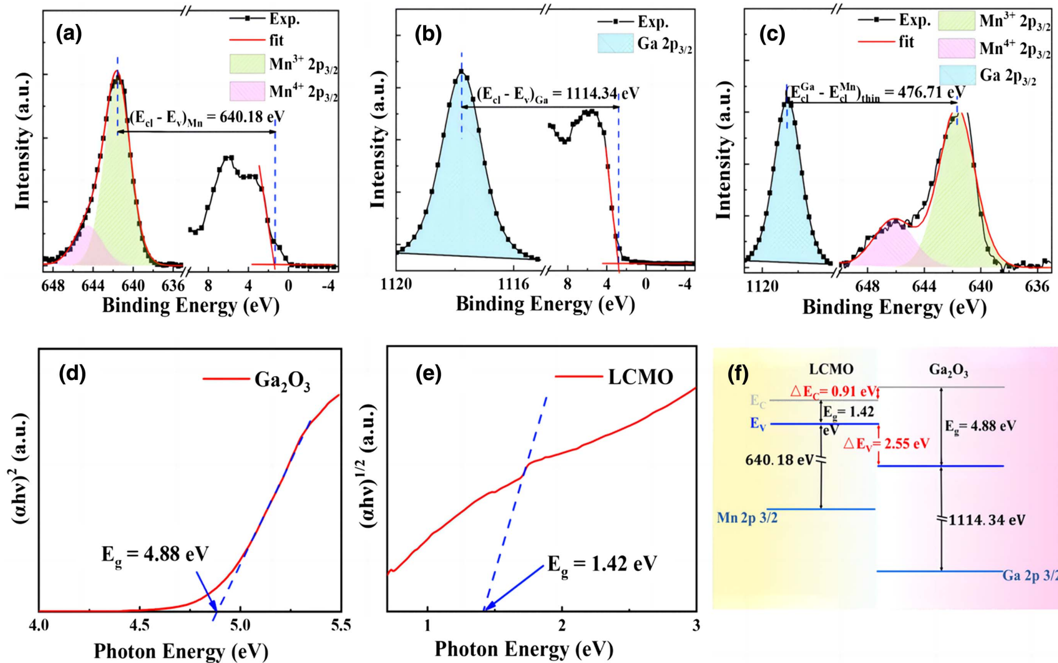

Fig. 5. CL and valence band XPS energy spectrum of (a) LCMO (∼100 nm)/STO and (b) Ga_2O_3 (∼300 nm)/LCMO (∼100 nm)/STO; (c) CL XPS energy spectrum of Ga_2O_3 (∼3 nm)/LCMO (∼100 nm)/STO sample; (d) bandgap of Ga_2O_3 film; and (e) LCMO film determined by Tauc plots method; (f) band alignment at the Ga_2O_3/LCMO pn junction.

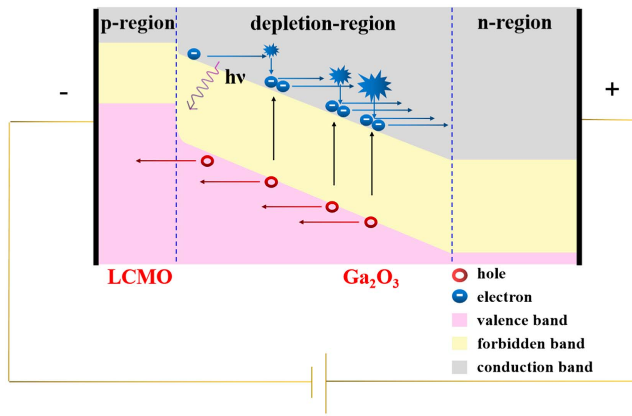

Fig. 6. Avalanche multiplication process of Ga_2O_3/LCMO APD.

determine the value of ΔE_c as 0.91 eV. These results are illustrated in the band alignment diagram of the Ga_2O_3/LCMO heterojunction in Fig. 5(f). The Ga_2O_3/LCMO pn junction exhibits a Type-I nested alignment with a large ΔE_v of 2.55 eV, which forms an effective barrier against hole injection in the Ga_2O_3 layer, resulting in a large space charge region in the heterojunction. The formed broader depletion region increases the carrier acceleration distance and promotes intense impact ionization.

When a reverse bias is applied to a Ga_2O_3/LCMO pn junction APD, migrations of holes from Ga_2O_3 to LCMO and electrons from LCMO to Ga_2O_3 occur simultaneously. This process is illustrated in Fig. 6. At low reverse bias, the built-in electric field in the space charge region of Ga_2O_3 blocks the photogenerated carriers generated upon the 254 nm UV irradiation. As the reverse bias voltage increases, the carriers gain more kinetic energy, which allows them to overcome the electric field barrier. By increasing the reverse bias, photon-induced charge carriers are accelerated and undergo cascade amplifications through impact ionization within the broader depletion layer. Such a multiplication process allows enhanced photoresponsivity and avalanche gain[29].

5. Conclusion

In summary, the epitaxial Ga_2O_3/LCMO pn junction exhibits outstanding photoelectric response characteristics in the solar-blind APD. The band alignment of the heterojunction was also studied to understand its avalanche breakdown mechanism. The nested arrangement of the band alignment results in a large valence band offset at the interface, which allows the photoexcited carriers to be accelerated by increasing the reverse bias. The designed APD incorporating epitaxial β-Ga_2O_3/LCMO pn junction exhibits a broader depletion region, contributing to a large responsivity of 568 A/W as well as an enhanced avalanche gain of up to 3.0×10^5 at a reverse bias voltage of 37.9 V. Moreover, Ga_2O_3 is an emerging WBG semiconductor for various applications of power electronics and optoelectronics. Thus, the capability of epitaxially integrating Ga_2O_3 with p-type semiconductor demonstrated in this work offers more opportunities to develop high-performance Ga_2O_3-based electronic and optoelectronic devices.

Acknowledgement

This work was supported by the National Natural Science Foundation of China (Nos. 12074044, 11874230, 52233014, and 12274243), the Fund of State Key Laboratory of Information Photonics and Optical Communications (No. IPOC2021ZT05), and the Fundamental Research Funds for the Central Universities (BUPT).

References

1. X. Chen, F. Ren, S. Gu, and J. Ye, "Review of gallium-oxide-based solar-blind ultraviolet photodetectors," Photonics Res. **7**, 381 (2019).
2. J. Chen, W. Ouyang, W. Yang, J. H. He, and X. Fang, "Recent progress of heterojunction ultraviolet photodetectors: materials, integrations, and applications," Adv. Funct. Mater. **30**, 1909909 (2020).
3. D. Kaur and M. Kumar, "A strategic review on gallium oxide based deep-ultraviolet photodetectors: recent progress and future prospects," Adv. Opt. Mater. **9**, 2002160 (2021).
4. X. Zhengyuan and B. M. Sadler, "Ultraviolet communications: potential and state-of-the-art," IEEE Commun. Mag. **46**, 67 (2008).
5. M. M. Fan, K. W. Liu, Z. Z. Zhang, B. H. Li, X. Chen, D. X. Zhao, C. X. Shan, and D. Z. Shen, "High-performance solar-blind ultraviolet photodetector based on mixed-phase ZnMgO thin film," Appl. Phys. Lett. **105**, 011117 (2014).
6. B. Liu, D. Chen, H. Lu, T. Tao, Z. Zhuang, Z. Shao, W. Xu, H. Ge, T. Zhi, F. Ren, J. Ye, Z. Xie, and R. Zhang, "Hybrid light emitters and UV solar-blind avalanche photodiodes based on III-nitride semiconductors," Adv. Mater. **32**, e1904354 (2020).
7. X. Hou, Y. Zou, M. Ding, Y. Qin, Z. Zhang, X. Ma, P. Tan, S. Yu, X. Zhou, X. Zhao, G. Xu, H. Sun, and S. Long, "Review of polymorphous Ga_2O_3 materials and their solar-blind photodetector applications," J. Phys. D **54**, 043001 (2021).
8. Y.-J. Lu, C.-N. Lin, and C.-X. Shan, "Optoelectronic diamond: growth, properties, and photodetection applications," Adv. Opt. Mater. **6**, 1800359 (2018).
9. Y. Yuan, W. Hao, W. Mu, Z. Wang, X. Chen, Q. Liu, G. Xu, C. Wang, H. Zhou, Y. Zou, X. Zhao, Z. Jia, J. Ye, J. Zhang, S. Long, X. Tao, R. Zhang, and Y. Hao, "Toward emerging gallium oxide semiconductors: a roadmap," Fundam. Res. **1**, 697 (2021).
10. S. J. Pearton, J. Yang, P. H. Cary, F. Ren, J. Kim, M. J. Tadjer, and M. A. Mastro, "A review of Ga_2O_3 materials, processing, and devices," Appl. Phys. Rev. **5**, 011301 (2018).
11. X. Hou, X. Zhao, Y. Zhang, Z. Zhang, Y. Liu, Y. Qin, P. Tan, C. Chen, S. Yu, M. Ding, G. Xu, Q. Hu, and S. Long, "High-performance harsh-environment-resistant GaO_x solar-blind photodetectors via defect and doping engineering," Adv. Mater. **34**, 2106923 (2022).
12. N. Liu, T. Zhang, L. Chen, J. Zhang, S. Hu, W. Guo, W. Zhang, and J. Ye, "Fast-response amorphous Ga_2O_3 solar-blind ultraviolet photodetectors tuned by a polar AlN template," IEEE Electron Device Lett. **43**, 68 (2022).
13. Y. Chen, Y. Lu, M. Liao, Y. Tian, Q. Liu, C. Gao, X. Yang, and C. Shan, "3D solar-blind Ga_2O_3 photodetector array realized via origami method," Adv. Funct. Mater. **29**, 1906040 (2019).
14. B. Qiao, Z. Zhang, X. Xie, B. Li, K. Li, X. Chen, H. Zhao, K. Liu, L. Liu, and D. Shen, "Avalanche gain in metal-semiconductor-metal Ga_2O_3 solar-blind photodiodes," J. Phys. Chem. C **123**, 18516 (2019).
15. W. Y. Kong, G. A. Wu, K. Y. Wang, T. F. Zhang, Y. F. Zou, D. D. Wang, and L. B. Luo, "Graphene-β-Ga_2O_3 heterojunction for highly sensitive deep UV photodetector application," Adv. Mater. **28**, 10725 (2016).
16. Y. Wang, Z. Yang, H. Li, S. Li, Y. Zhi, Z. Yan, X. Huang, X. Wei, W. Tang, and Z. Wu, "Ultrasensitive flexible solar-blind photodetectors based on

graphene/amorphous Ga_2O_3 van der Waals heterojunctions," ACS Appl. Mater. Interfaces **12**, 47714 (2020).
17. Y. Wang, Y. Tang, H. Li, Z. Yang, Q. Zhang, Z. He, X. Huang, X. Wei, W. Tang, W. Huang, and Z. Wu, "p-GaSe/n-Ga_2O_3 van der Waals heterostructure photodetector at solar-blind wavelengths with ultrahigh responsivity and detectivity," ACS Photonics **8**, 2256 (2021).
18. Z. Wu, L. Jiao, X. Wang, D. Guo, W. Li, L. Li, F. Huang, and W. Tang, "A self-powered deep-ultraviolet photodetector based on an epitaxial Ga_2O_3/Ga:ZnO heterojunction," J. Mater. Chem. C **5**, 8688 (2017).
19. Y. Wang, W. Cui, J. Yu, Y. Zhi, H. Li, Z. Y. Hu, X. Sang, E. J. Guo, W. Tang, and Z. Wu, "One-step growth of amorphous/crystalline Ga_2O_3 phase junctions for high-performance solar-blind photodetection," ACS Appl. Mater. Interfaces **11**, 45922 (2019).
20. B. Zhao, F. Wang, H. Chen, Y. Wang, M. Jiang, X. Fang, and D. Zhao, "Solar-blind avalanche photodetector based on single ZnO–Ga_2O_3 core–shell microwire," Nano Lett. **15**, 3988 (2015).
21. Y. Wang, H. Li, J. Cao, J. Shen, Q. Zhang, Y. Yang, Z. Dong, T. Zhou, Y. Zhang, W. Tang, and Z. Wu, "Ultrahigh gain solar blind avalanche photodetector using an amorphous Ga_2O_3-based heterojunction," ACS Nano **15**, 16654 (2021).
22. X. Chen, Y. Xu, D. Zhou, S. Yang, F. F. Ren, H. Lu, K. Tang, S. Gu, R. Zhang, Y. Zheng, and J. Ye, "Solar-blind photodetector with high avalanche gains and bias-tunable detecting functionality based on metastable phase alpha-Ga_2O_3/ZnO isotype heterostructures," ACS Appl. Mater. Interfaces **9**, 36997 (2017).
23. Q. Zhang, N. Li, T. Zhang, D. Dong, Y. Yang, Y. Wang, Z. Dong, J. Shen, T. Zhou, Y. Liang, W. Tang, Z. Wu, Y. Zhang, and J. Hao, "Enhanced gain and detectivity of unipolar barrier solar blind avalanche photodetector via lattice and band engineering," Nat. Commun. **14**, 418 (2023).
24. W. E. Mahmoud, "Solar blind avalanche photodetector based on the cation exchange growth of β-Ga_2O_3/SnO_2 bilayer heterostructure thin film," Sol. Energy Mater. Sol. Cells **152**, 65 (2016).
25. M. B. Salamon and M. Jaime, "The physics of manganites: structure and transport," Rev. Mod. Phys. **73**, 583 (2001).
26. J. M. D. Coey, M. Viret, and S. von Molnár, "Mixed-valence manganites," Adv. Phys. **48**, 167 (1999).
27. Z. Liao, M. Huijben, Z. Zhong, N. Gauquelin, S. Macke, R. J. Green, S. Van Aert, J. Verbeeck, G. Van Tendeloo, K. Held, G. A. Sawatzky, G. Koster, and G. Rijnders, "Controlled lateral anisotropy in correlated manganite heterostructures by interface-engineered oxygen octahedral coupling," Nat. Mater. **15**, 425 (2016).
28. J. Yu, Y. Wang, H. Li, Y. Huang, W. Tang, and Z. Wu, "Tailoring the solar-blind photoresponse characteristics of β-Ga_2O_3 epitaxial films through lattice mismatch and crystal orientation," J. Phys. D **53**, 24LT01 (2020).
29. S. O. Kasap, *Optoelectronics and Photonics: Principles and Practices*, 2nd ed. (Pearson, 2012).
30. M.-Q. Li, N. Yang, G.-G. Wang, H.-Y. Zhang, and J.-C. Han, "Highly preferred orientation of Ga_2O_3 films sputtered on SiC substrates for deep UV photodetector application," Appl. Surf. Sci. **471**, 694 (2019).
31. G. C. Hu, C. X. Shan, N. Zhang, M. M. Jiang, S. P. Wang, and D. Z. Shen, "High gain Ga_2O_3 solar-blind photodetectors realized via a carrier multiplication process," Opt. Express **23**, 13554 (2015).
32. G. Greczynski and L. Hultman, "X-ray photoelectron spectroscopy: towards reliable binding energy referencing," Prog. Mater Sci. **107**, 100591 (2020).
33. Z. Liu, J. Yu, P. Li, X. Wang, Y. Zhi, X. Chu, X. Wang, H. Li, Z. Wu, and W. Tang, "Band alignments of β-Ga_2O_3 with MgO, Al_2O_3 and $MgAl_2O_4$ measured by X-ray photoelectron spectroscopy," J. Phys. D **52**, 295104 (2019).